Sciences du Nord Nature Science and Technology
Vol. 2, No. 02, December 2025: pp. 132-144
E-ISSN: 3046-6504
P-ISSN: 3047-4922
DOI: https://doi.org/10.71238/snnst.v1i02.233

Hydrogen-Embrittlement-Aware Crack Evolution Modeling for Additively Manufactured Pressure-Bearing Components: A Systematic Review

Rupesh Ramesharo Dhore [1]
[1] Senior Design Release Engineer Solize USA Corporation Canton, MI, USA
Coresponding Author: rupeshdhorey@gmail.com

ARTICLE HISTORY
Received July, 2025 **Revised Oct, 2025** **Accepted Dec, 2025**

ABSTRACT

The unique microstructures, defect populations, and residual stresses created by Additively Manufactured (AM) metallic components make prediction of hydrogen-assisted cracking highly complex and require more research. This systematic review collates 22 sources from the AM process science, hydrogen embrittlement (HE) mechanisms, experimental data on AM alloys and phase field fracture theory in a coherent framework to develop crack evolution modelling of AM pressure-bearing components accounting for HE. Stress-assisted multi-trap hydrogen transport is combined with Taylor-based crack-tip hardening models, first-principles-informed fracture energy degradation models, regularised phase field fracture models and hydrogen-accelerated fatigue models and tested against reported benchmarks. The synthesis indicates that hydrogen charging at −50 °C did not significantly affect the ductility of the conventionally manufactured 316L but did cause the hot isostatically pressed AM 316L to have almost double the ductility, the elongation based embrittlement index of laser powder bed fused 316L lattices increased from approximately 4.0% to 17.6% as the thickness of the struts increased from 0.6 to 1.4 mm, and hydrogen caused the rate of fatigue crack propagation in heat-treated laser powder bed fused Inconel 718 to increase by a factor of 2.8. Damage coefficients of 0.89, 0.67, and 0.41 are used for the degradation laws of the iron, aluminium, and nickel anchor, while explicit consideration of the evolution of hydride and Ti3Al has to be made for electron beam melted Ti-6Al-4V between 0.29 and 0.90 wt.% hydrogen. The major barriers are: (1) unmeasured trap energetics in printed microstructures, (2) limited gaseous-hydrogen fatigue data, and (3) lack of qualifying criteria based on simulations.

Keywords: *316L Stainless Steel; Additive Manufacturing; Crack Evolution; Fatigue Crack Growth; Hydrogen Embrittlement; Hydrogen Trapping; Phase fFeld Fracture; Pressure-Bearing Components; Strain Gradient Plasticity*

INTRODUCTION

The move to hydrogen-based energy systems has revived the demand for the structural integrity of metallic components that store, transport or control pressurised hydrogen, such as storage vessels, valves, manifolds, and heat-exchanger bodies. Additive manufacturing (AM), which is the process of consolidating feedstock (one by one) to manufacture near-net-shape components, is viewed as an option for such parts, as it can produce complex geometries with a minimum lead time. Four conditions of the post-build material, as-built, annealed, hot isostatically pressed (HIP) and HIP and 30% cold work, have been investigated at room temperature and −50 °C, and the HIP condition exhibited nearly twice the ductility of conventionally manufactured (CM) 316L after hydrogen charging at −50 °C [1].

Hydrogen embrittlement (HE) is a reduction of ductility, toughness and fatigue properties that is a result of the presence of atomic hydrogen. Mechanical and cyclic test data for AM materials have been critically appraised and have revealed a significant difference between the response of

AM materials and wrought material, particularly for titanium alloys, nickel superalloys, and austenitic stainless steels [2] and that the effect is less than for CM material in several alloy systems. Hydrogen accumulation at phase interfaces, where a critical local concentration is reached, has been found to be the main cause of hydrogen induced crack initiation (HICI) in AM microstructures and the presence of porosity and its interaction with the surrounding matrix is not yet fully characterized. Predictive tools that are tailored for wrought alloys can't be applied to 3-D printed components without adjustments.

Predictive modelling of crack evolution under hydrogen exposure has now come a long way with the phase field fracture approach, a variational approach that involves a diffuse scalar damage field to represent a sharp crack. The most general formulations now allow these four order parameters displacement field, corrosion order parameter, concentration of metal ions, and fracture order parameter to be solved in a single electro-chemo-mechanical framework, yielding the transition between anodic dissolution and hydrogen-driven cracking from the environment, instead of being prescribed [3]. In this context, this review brings together process science, hydrogen–metal interaction data and multi-physics fracture theory into a unified approach for modelling the evolution of cracks in AM pressure-bearing components that is capable of capturing the influence of hydrogen, and the parameters, validation data, and research gaps governing the use of this approach are identified.

LITERATURE REVIEW

2.1 Process–Structure Foundations of AM Pressure-Bearing Components

The thermal history imposed by the moving heat source is a direct result of the microstructure that is encountered by hydrogen in a printed component. Process–structure–property analysis has revealed steep temperature gradient, high cooling rate, which is typically in the range of 103 to 106 K s−1, repeated re-melting of deposited layers, epitaxial columnar grain growth along the build direction, and high residual stresses in the fusion-based AM process [4]. All features are important for hydrogen: columnar grain boundaries act as oriented diffusion paths, solidification cell walls contain dislocations that act as traps, and residual tensile stresses increase the hydrostatic stress that increases hydrogen concentrations. Table 1 collates the main process characteristics affecting hydrogen susceptibility in the two major routes for powder bed processing.

Table 1. Process Attributes of Powder Bed Fusion Routes Relevant to Hydrogen Susceptibility

Attribute	Laser powder bed fusion (LPBF)	Electron beam melting (EBM)
Heat source and atmosphere	Fibre laser, inert gas	Electron beam, vacuum
Typical powder size	15–45 μm	45–105 μm
Typical layer thickness	20–100 μm	50–200 μm
Thermal regime	Near-ambient build plate; very rapid cooling	Elevated build temperature; Ti-6Al-4V melted at about 1900 °C and held near 700 °C
Characteristic microstructure	Cellular sub-grains, columnar grains, high dislocation density	Columnar prior-β grains, fine α plates about 0.2 μm wide

Dominant defects	Lack-of-fusion and keyhole pores, high residual stress	Gas porosity, rough surfaces, lower residual stress
Hydrogen-relevant implication	Dense trap population at cell walls; anisotropic transport	Phase interfaces and hydride-forming β and α'' phases

Source: Compiled and synthesised from the reviewed literature.

2.2 Hydrogen-Assisted Fatigue Crack Growth in AM Alloys

Pressure-bearing components, in particular, are typically not subjected to monotonous loading - pressurisation cycles are likely to cause appreciable fatigue loading, where hydrogen effects are likely to be most severe. For the in situ electrochemical charging of Inconel 718, hydrogen caused a significant increase in the FCGR, and the acceleration of FCGR was up to 2.8 times for the post-heat-treated condition [5]. Pathways for rapid diffusion along grain boundaries were formed, leading to hydrogen enrichment in local regions of the material created by planar dislocation slip, which resulted in extensive intergranular cracking and suppression of dislocation emission resulting in restricted plasticity ahead of the crack tip. Therefore, any credible model for the crack evolution of AM nickel alloys needs to be coupled with the reduction in plastic shielding of the crack-tip, not just hydrogen as a reduction in static toughness.

2.3 Mechanistic and Characterisation Frameworks

There is a solid body of theory for modelling hydrogen uptake, lattice diffusion, trapping at microstructural defects, and subsequent degradation of cohesion and plastic flow for modelling gaseous HE. It is a well-known transport model for lattice hydrogen in stressed solids to describe transport as a mass balance, including a Fickian term and a term related to the gradient of the hydrostatic stress, as shown in Equation (1) [6]. Here, C is the lattice hydrogen concentration, D is the diffusion coefficient, VH is the partial molar volume of hydrogen, R is the gas constant, T is the absolute temperature and σh is the hydrostatic stress. Since the hydrogen incident on the blunting crack is concentrated at a finite distance ahead of the crack, Equation (1) gives accurate predictions for hydrogen enrichment at the point where fracture begins.

$$\frac{\partial C}{\partial t} + \nabla \cdot \left[-D\nabla C + \frac{D\overline{V}_{\mathrm{H}} C}{RT} \nabla \sigma_{\mathrm{h}} \right] = 0 \quad (1)$$

Experimental quantities which are the basis for the characterisation literature for the purpose of validating crack evolution models. Slow strain rate tensile (SSRT) testing, fracture mechanics testing for threshold stress intensity factors (Kth) and crack growth resistance and fatigue crack growth testing under pressurised hydrogen conditions have been established and applied to ferritic steels, austenitic stainless steels, nickel alloys and titanium alloys for gaseous HE [7].

It is emphasised that the compatibility of all stainless steels is good, but that the high strength steels and precipitation hardened nickel alloys have high sensitivity. These differences are carried over to AM where the same alloy classes are used for pressure applications, but they have different populations of defects and phase stability.

METHODS

A representative sample of 22 publications, including experimental research, critical reviews, monographs and theoretical modelling papers between 2010 and 2024 were selected and included in a curated corpus to which a systematic review protocol was applied. The sources were grouped into four clusters; the AM taxonomy used follows that of the existing classification of

powder bed and directed energy deposition processes, and their characteristic densities, anisotropy, and residual stress states [8]. Each source of information was used to extract governing equations, material parameters, test conditions, and quantitative results and results were cross tabulated. Table 2 relates the literature to the conceptual building blocks of the framework and Figure 1 shows the resulting modelling architecture.

Table 2. Literature Mapping Matrix Linking the Reviewed Sources to Framework Components

Framework component	Sources	Contribution to the framework
AM process–structure–property	[4], [8], [9], [10]	Thermal history, defects, residual stress, fatigue drivers
HE mechanisms	[11], [12], [13], [14]	HEDE, HELP, AIDE, hydride formation, model classes
Gaseous HE theory and testing	[6], [7]	Transport and trapping theory, test methods, alloy classes
HE data on AM alloys	[1], [2], [5], [15], [16]	Calibration and validation benchmarks
Phase field fracture theory	[17], [18], [19]	Regularised fracture, irreversibility, solution schemes
Hydrogen-sensitive phase field	[3], [20], [21], [22]	Coupled transport–plasticity–fracture formulations

Source: Compiled and synthesised from the reviewed literature.

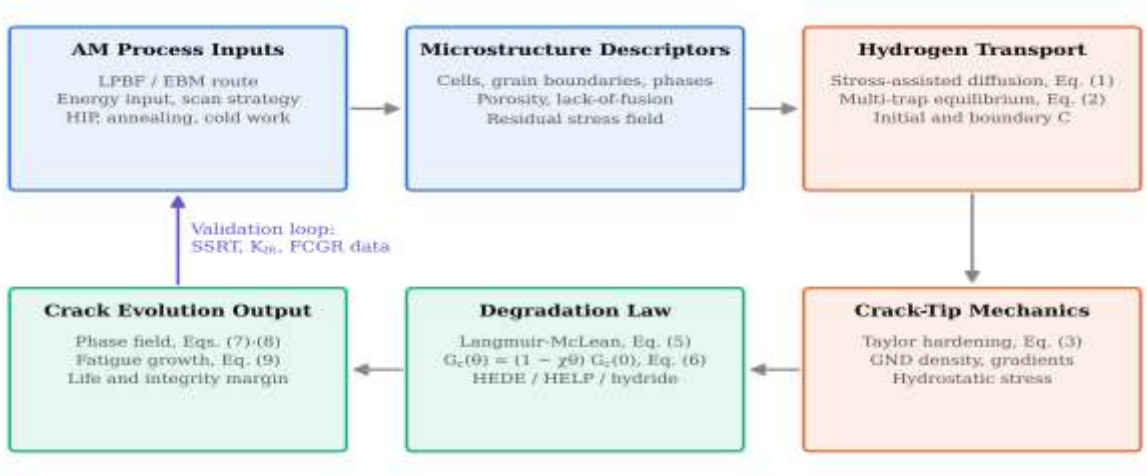


Figure 1. Integrated Modelling Architecture for Hydrogen-Embrittlement-Aware Crack Evolution in AM Pressure-Bearing Components

RESULTS AND DISCUSSION

4.1 Hydrogen Transport and Trapping Formulations

The hydrogen concentration obtained from lattice diffusion is too low to account for the amount of hydrogen observed in AM microstructures that have high densities of dislocations, cell walls, grain boundaries, and interfaces. Multi-trap is a formulation in which hydrogen is distributed between lattice sites and traps according to the Oriani equilibrium, Equation (2), where θL and θT are the occupancies of the lattice sites and traps, respectively, and WB is the binding energy of the

trap state [9]. In the mechanism-based variant, the dislocation trap density is function of plastic deformations as described by Equation (3), which is known as the Taylor hardening model, with M being the Taylor factor, α an empirical coefficient, μ the shear modulus, b the Burgers vector, and ϱS and ϱG the statistically stored and geometrically necessary dislocation densities, respectively. This coupling increases the tensile stress, hydrogen concentration and number of traps in the first few tens of micrometres around the crack tip.

$$\frac{\theta_{\mathrm{T}}}{1-\theta_{\mathrm{T}}} = \frac{\theta_{\mathrm{L}}}{1-\theta_{\mathrm{L}}} \exp\left(\frac{W_{\mathrm{B}}}{RT}\right) \quad (2)$$

$$\sigma_{\mathrm{flow}} = M\alpha\mu b\sqrt{\rho_{\mathrm{S}} + \rho_{\mathrm{G}}} \quad (3)$$

4.2 Experimental Benchmarks from AM Alloys

Validating quantitative benchmarks are available from tensile testing of LPBF 316L auxetic lattices with strut thicknesses of 0.6, 1.0 and 1.4 mm, electrochemically charged in NaOH solution for 24 h at 80 °C and strained at 4 × 10−5 s−1 [10]. Susceptibility is represented by the embrittlement index given by Equation (4). For the 0.6 mm struts, strength fell from 340 to 320 MPa and uniform elongation from 17.4% to 16.7%, whereas the 1.4 mm struts fell from 550 to 523 MPa and from 29% to 23.9%. As a result, the elongation index increased from ~4.0% to 17.6% for thickness, together with the appearance of cleavage facets and increased twinning, as illustrated in Figure 2 and Table 3.

$$I_{\mathrm{HE}} = \frac{\varepsilon_{\mathrm{air}} - \varepsilon_{\mathrm{H}}}{\varepsilon_{\mathrm{air}}} \times 100\% \quad (4)$$

Table 3. Quantitative Hydrogen Effects Reported for Additively Manufactured Alloys

Alloy and process	Hydrogen exposure	Test method	Key quantitative outcome
316L, LPBF (as-built, annealed, HIP, HIP + 30% cold work)	Hydrogen pre-charging	Uniaxial tension at room temperature and −50 °C	HIP ductility about 2× that of CM 316L at −50 °C; cold-worked AM yield strength about 2× with comparable ductility
316L auxetic lattice, LPBF, 70 J mm^{-3}	NaOH, 24 h, 80 °C	SSRT, 4 × 10^{-5} s^{-1}	1.4 mm strut: 550 to 523 MPa, 29% to 23.9% elongation
Inconel 718, SLM	In situ electrochemical charging	Fatigue crack growth	FCGR increased up to 2.8× in the post-heat-treated condition
Ti-6Al-4V, EBM	Gaseous hydrogenation at 650 °C	XRD, SEM, TEM, hardness	Ti$_3$Al at 0.29 wt.%; δ hydrides at 0.58 wt.%; hardness decreases with hydrogen

Source: Compiled and synthesised from the reviewed literature.

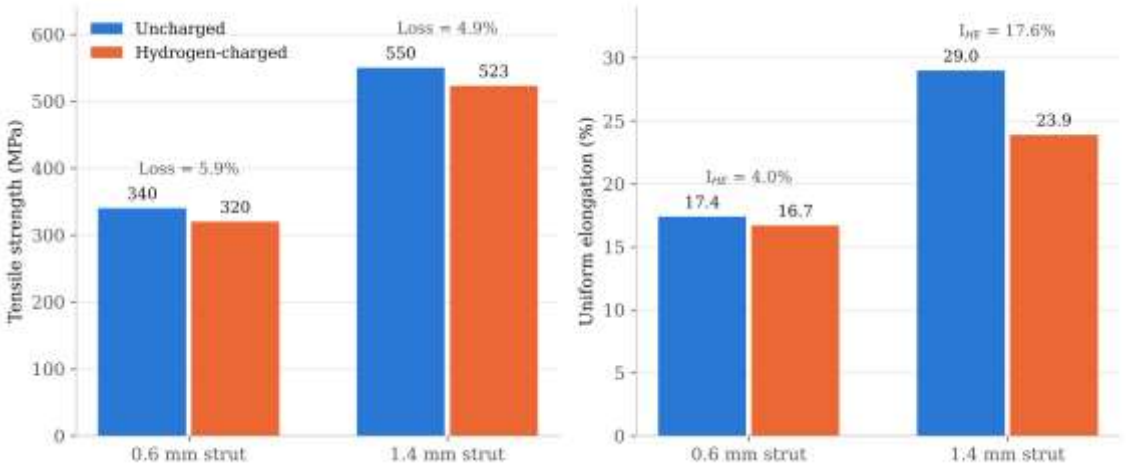


Figure 2. Tensile Strength and Uniform Elongation of LPBF 316L Auxetic Lattices Before and After Hydrogen Charging

4.3 Gradient Plasticity and Crack-Tip Hydrogen Enrichment

The conventional theory of plasticity only predicts a few times the yield strength for crack-tip hydrostatic stresses, which are not enough to account for decohesion in ductile alloys. Geometrically necessary dislocations created by high plastic strain gradients close to the tip increase the stresses, hydrogen concentration, and, consequently, the reduction of fracture energy in the region of micrometres around the tip, which resolves this contradiction [21] for gradient-based formulations that incorporate stress-assisted diffusion, strain gradient plasticity, and hydrogen-sensitive phase field description. These models reproduced the transition to brittle fracture in otherwise ductile metals, captured sensitivity of the plastic and fracture length scales, loading rate, and hydrogen content, and agree with threshold stress intensity measurements over a wide range of applied potentials for the ultra-high-strength steel AerMet100.

4.4 Mechanism Selection for Degradation Laws

The degradation law used assumes the mechanism for embrittlement that is operating. Critical surveys of HE phenomena differentiate between four mechanisms: hydrogen-enhanced decohesion (HEDE), hydrogen-enhanced localised plasticity (HELP), adsorption-induced dislocation emission (AIDE) and stress-induced hydride formation, and the results indicate that more than one of these mechanisms is typically active, depending on the alloy, microstructure, hydrogen concentration, and loading conditions [11]. In the case of AM parts, this plurality is consequential: cellular austenitic structures promote localised plasticity, precipitation hardened nickel alloys tend to intergranular fracture with decohesion, and titanium alloys have a potential for hydride formation. Table 4 makes the link between each mechanism and its continuum representation and the AM alloy classes to which it is most applicable.

Table 4. Hydrogen Embrittlement Mechanisms and Their Continuum Representation in Crack Evolution Models

Mechanism	Physical basis	Continuum representation	Most relevant AM alloys
HEDE	Reduced atomic cohesion at boundaries and interfaces	Fracture energy degradation $G_c(\theta)$	Inconel 718, high-strength steels
HELP	Enhanced dislocation mobility and slip localisation	Hydrogen-dependent flow stress or softening law	316L and other austenitic steels
AIDE	Surface adsorption easing dislocation emission at the tip	Modified crack-tip surface energy	Near-surface regions of most alloys
Hydride formation	Precipitation of brittle hydride phases	Additional phase or transformation field	Ti-6Al-4V and other titanium alloys
HELP-mediated HEDE	Localised plasticity enriches hydrogen, then decohesion	Gradient plasticity coupled with $G_c(\theta)$	As-built LPBF 316L, Inconel 718

Source: Compiled and synthesised from the reviewed literature.

4.5 Hydrogen-Sensitive Phase Field Fracture

The basic scheme for the phase field order parameter is coupled with displacements, and the concentration of hydrogen is coupled with the phase field in an implicit manner, while the fracture energy degradation is based on first principles calculations. The Langmuir–McLean isotherm, Equation (5), is used to obtain the surface coverage θ and the critical energy release rate decays linearly with coverage as given by Equation (6) [22]. As shown in Table 5, the damage coefficient (χ) calculated from the density functional theory are 0.89 for Fe, 0.67 for Al and 0.41 for Ni. The resulting degradation curves in Figure 3 reveal that fracture resistance is significantly reduced for iron-based alloys at relatively small concentrations, similar to the cracking that was experienced at one-tenth of the anticipated fracture toughness.

$$\theta = \frac{C}{C+\exp\left(-\frac{\Delta g_b^0}{RT}\right)} \tag{5}$$

$$G_c(\theta) = (1-\chi\theta)G_c(0) \tag{6}$$

Table 5. Representative Parameters of Hydrogen-Sensitive Phase Field Fracture Models

Parameter	Symbol	Value	Basis
Damage coefficient, iron	χ	0.89	First-principles (DFT) fit
Damage coefficient, aluminium	χ	0.67	First-principles (DFT) fit
Damage coefficient, nickel	χ	0.41	First-principles (DFT) fit, Σ3 and Σ5 boundaries

Segregation energy at interfaces	Δg_b^0	30 kJ mol^{-1}	Benchmark value for iron-based alloys
Partial molar volume of hydrogen	V_H	2000 mm^3 mol^{-1}	Iron-based alloys
Gas constant	R	8.314 J mol^{-1} K^{-1}	Physical constant
Reference temperature for Figure 3	T	300 K	Ambient service condition

Source: Compiled and synthesised from the reviewed literature.

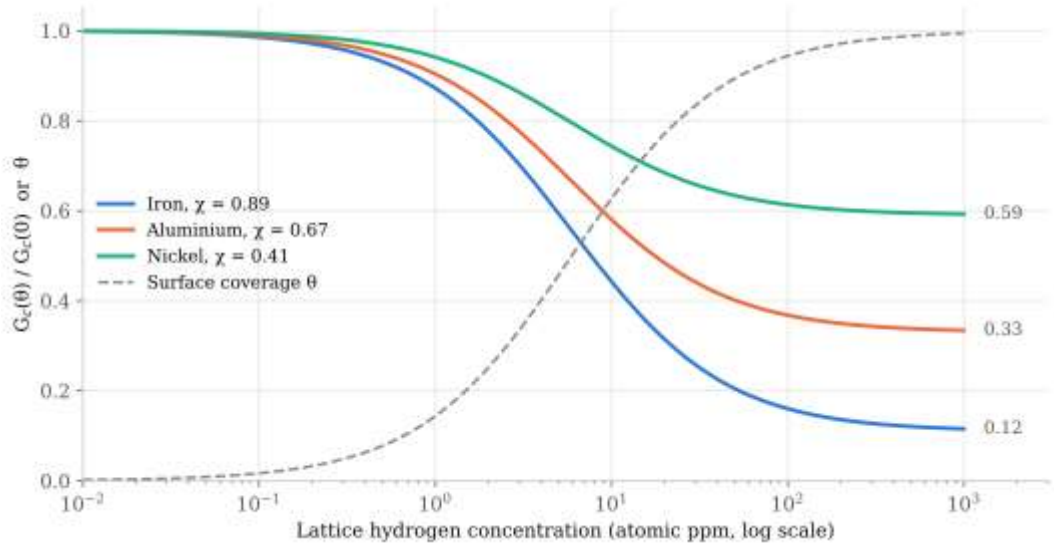


Figure 3. Hydrogen-Dependent Degradation of Critical Energy Release Rate for Iron, Aluminium, and Nickel Computed from Equations (5) and (6)

The phase field fracture regularises the topology of sharp cracks over a length scale ℓ and converts the Griffith energy balance into the minimisation of the functional in Equation (7), where the phase field ϕ is either 0 for the undamaged material or 1 for the fully damaged material, the undamaged strain energy density is denoted by ψ0, and the small residual stiffness is denoted by k [17]. Strong implementation separates the strain energy into tensile and compressive components, with the latter set to zero, so that no energy is provided by compression forces for cracking, and adds a history field $\mathcal{H}$ that is the highest tensile energy ever seen at a material point to ensure irreversibility. The operator-split, or staggered, algorithm of the displacement and phase field subproblems is still the most popular solution method that has been used in the hydrogen coupled implementations due to the linearity and convexity of each subproblem.

$$\Psi = \int_\Omega [(1-\varphi)^2 + k]\psi_0(\varepsilon)dV + \int_\Omega G_c(\theta)\left(\frac{\varphi^2}{2\ell} + \frac{\ell}{2}|\nabla\varphi|^2\right)dV \quad (7)$$

The thermodynamic consistency of this approach can be obtained by deriving the governing equations from the variational principles, where the dissipation inequality is fulfilled as a result of the irreversibility constraint for the phase field and multi-field finite element implementations couple the displacement and phase field as two primary unknowns [18]. The local evolution law of Equation (8) is obtained from the stationarity of Equation (7) with respect to φ, the history field, representing the instantaneous tensile energy. If Gc depends on θ via Equation (6), additional

nucleation, propagation, branching and coalescence follow naturally and no further criterion for driving the balance of the crack is necessary. This property is beneficial for AM parts where the location of any pores, surface roughness or lattice nodes from which a crack could form are unpredictable.

$$G_c(\theta)\left(\frac{\varphi}{\ell} - \ell\nabla^2\varphi\right) - 2(1-\varphi)\mathcal{H} = 0 \quad (8)$$

4.6 Microstructure-Specific Inputs from AM

The hydrogen problem is redefined with AM-specific phase, as is exemplified by the case of titanium alloys. Hydrogenated Ti-6Al-4V samples with an initial hydrogen content of 0.29, 0.58 and 0.90 wt.% made by electron beam melting (EBM) exhibited an initial structure consisting of α plates with a width of 0.2 μm, β plates and globular grains, and metastable α'' and ω phases [16]. At 0.29 wt.%, Ti3Al grew in size and proportion and co-precipitated nano-sized δ hydrides; at 0.90 wt.%,Ti3Al decayed into nanocrystal alongside with an increase in the proportion and size of hydrides, and the hardness of Ti3Al decreased with increasing hydrogen content. This evolution is shown in figure 4 indicating that a single degradation coefficient is insufficient for AM components produced from titanium alloys that form hydrides.

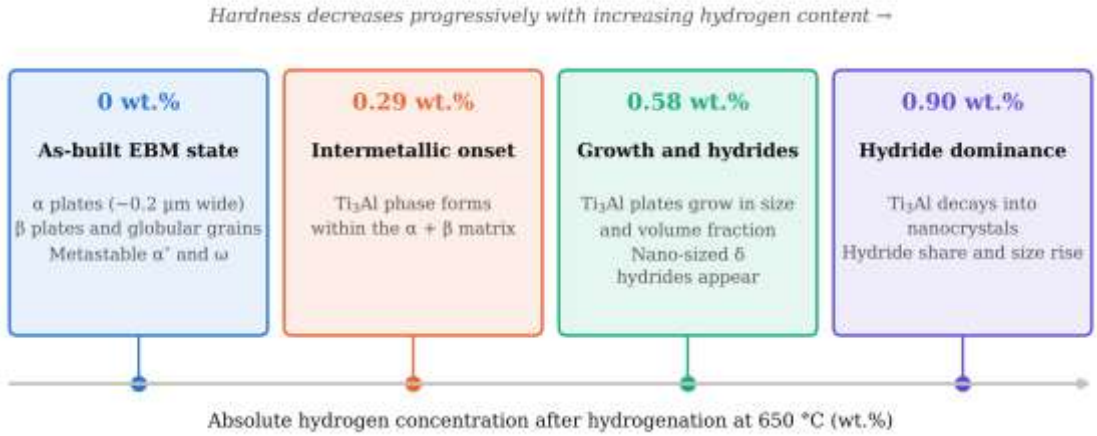


Figure 4. Hydrogen-Induced Phase Evolution in Electron Beam Melted Ti-6Al-4V as a Function of Hydrogen Concentration

The focus for austenitic and Ni-based AM alloys is different. It is generally concluded that the synergy found in many alloys for HE is that hydrogen-enhanced plasticity forms dense dislocation structures and enriches the local regions in hydrogen, followed by decohesion along slip bands or boundaries until fracture occurs [12]. This HELP-mediated HEDE sequence is adopted here for the coupled formulation in which the Taylor relation (3) describes the dislocation-induced stress elevation and the formation of traps, and the loss of cohesion is described by (6). Therefore, the high dislocation density and cellular walls that remain in the as-built LPBF microstructures contribute to both the hardening effect and H-trapping effect, and the latter effect is gradually reduced with subsequent annealing or HIP.

The rest of the inputs are provided by process metallurgy. The literature on the metallurgy and processing science of metal AM reveals that the porosity, chemical segregation, phase content, and residual stress of AM parts are a function of the power and the AM scan strategy, as well as the build temperature, and that a vacuum electron beam environment is not the same as an inert-gas laser AM environment in terms of elemental evaporation and contamination [9]. Porosity and lack-

of-fusion defects may be explicitly modeled as a geometric feature or as an initial phase field damage in the model; segregation at cell boundaries may be modeled as an elevated trap density; initial hydrostatic stress field entering the modelling of Equation (1) may be used to model residual stress. However, one main opportunity for process-aware integrity assessment is to be able to calibrate these inputs from process parameters, instead of from post mortem measurement.

4.7 Model Classification and Computational Considerations

It is important to note that the broad surveys of HE models and classifications have highlighted that hydrogen concentrations can progressively reach embrittling levels in high-strength materials with concentrations below 1 ppm [13]. The sensitivity has two implications with respect to pressure bearing AM parts. First, the initial concentration field produced during processing, surface finishing, or during electrochemical exposure could be a source of contamination for a component before it is exposed to service, and the initial field must be considered as an input to a model. Secondly, the degradation curves that are shown in Figure 3 are very steep at low concentrations; this leads to large uncertainties in the predicted crack initiation life when small uncertainties are present in the trapping parameters, so motivating the need for probabilistic calibration of the transport and degradation parameters.

There have been extensive reviews of phase field fracture that document the numerical requirements that govern the cost and accuracy. The length scale ℓ has to be captured by a mesh that is much finer than ℓ in the fracture process zone, and whether ℓ is a regularisation parameter or a material parameter related to strength is a modelling choice [19]. Monolithic and staggered solvers provide a balance between robustness and efficiency and the alternative geometric crack functions and degradation functions modify the pre-cracking response. Table 6 shows a physics-to-trapping-to-plasticity-to-validation-to-explicit physics coupling evolution of representative formulations.

Table 6. Comparative Capabilities of Phase Field Formulations for Hydrogen-Assisted Cracking

Formulation	Primary fields	Plasticity	Hydrogen trapping	Validation basis
Brittle variational phase field	u, φ	None (elastic)	Not included	Benchmark fracture problems
Hydrogen phase field with Langmuir–McLean degradation	u, φ, C	Elastic or J_2 flow	Lattice only	Notched specimens, cracking thresholds, pit-initiated cracks
Gradient-plastic hydrogen phase field	u, φ, C	Strain gradient plasticity	Lattice only	K_{th} of AerMet100 versus applied potential
Mechanism-based multi-trap phase field	u, φ, C_L, C_T	Taylor-based gradient plasticity	Multiple trap types	Notch tensile strength versus hydrogen content

Multi-phase-field SCC and HE theory	u, φ, corrosion field, metal ions, C	J_2 flow	Lattice only	Benchmark tests and seminal SCC experiments

Source: Compiled and synthesised from the reviewed literature.

4.8 Cyclic Loading of Pressure-Bearing Components

Most pressure-bearing components are governed by fatigue and the AM fatigue performance is dominated by porosity, lack-of-fusion defects, surface roughness, residual stress, and microstructural anisotropy; HIP and surface machining are identified as effective avenues for mitigation [10]. If the material is a defect tolerant material, then the Paris law of Equation (9) applies for crack growth developing from these defects, the hydrogen is included as an acceleration factor, αH, and CP and m are material constants. Figure 5 shows that the factor of 2.8 for heat-treated SLM Inconel 718 also shifts the growth curve and the calculated propagation life of a crack that has already grown from a defect under the same loading condition to approximately 0.36 of the inert life.

$$\frac{da}{dN} = \alpha_{\mathrm{H}} C_{\mathrm{P}} (\Delta K)^{\mathrm{m}} \tag{9}$$

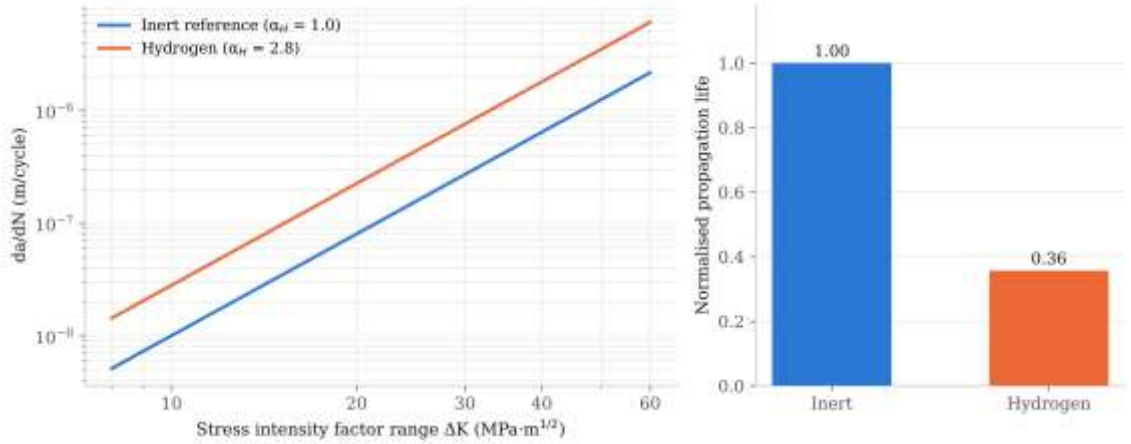


Figure 5. Hydrogen-Accelerated Paris-Regime Fatigue Crack Growth and Normalised Propagation Life for an Acceleration Factor of 2.8

4.9 Evolutionary Trends and Outlook

Multiscale characterisation, quantitative hydrogen mapping and predictive modelling are identified as the key frontier of the coupling of the three together with alloy design and standardised testing methods suitable for hydrogen service as part of comprehensive assessments of the materials challenge [14]. Figure 6 summarizes the evolution of the field from variational phase field fracture, to first-principles-informed hydrogen degradation and gradient plasticity, and to multi-trap and multi-mechanism formulations and to the first systematic AM-specific HE datasets. The major challenges to deployment for AM pressure equipment include the lack of trap binding energies measured on printed microstructures, limited fatigue data in gaseous hydrogen and the absence of qualification standards that accept simulation-based evidence.

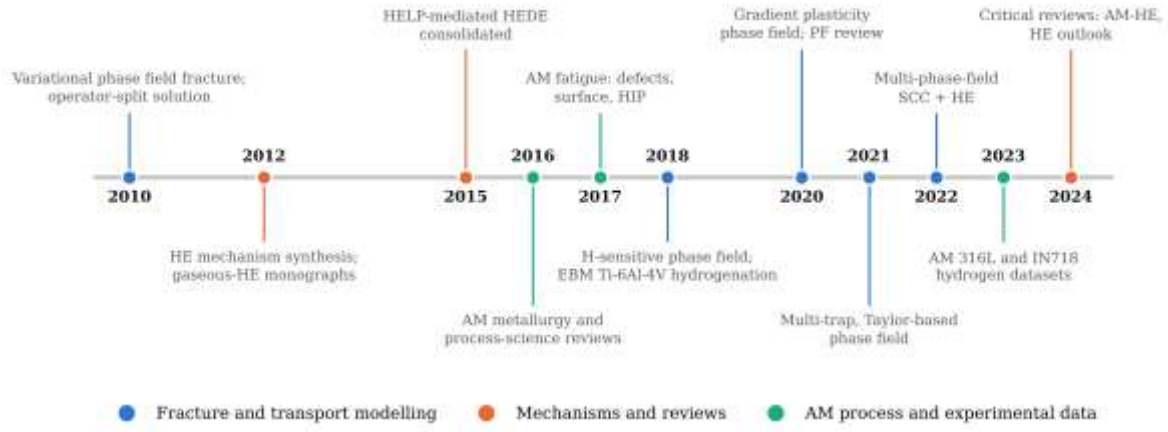


Figure 6. Evolutionary Timeline of Hydrogen-Assisted Fracture Modelling and AM Hydrogen Embrittlement Research

.

CONCLUSION

This systematic review shows that it is necessary to combine 4 factors to embed into a crack evolution modelling framework for AM pressure-bearing components that takes hydrogen embrittlement effects into account: process-derived microstructural descriptors, stress-assisted multi-trap hydrogen transport, mechanism-consistent degradation of fracture resistance, and regularised phase field fracture extended to cyclic loading. However, it is seen that these alloys are not always more susceptible than wrought alloys; for instance, the HIP treated 316L exhibited almost double the ductility of the conventional material at -50 °C and the SLM Inconel 716 exhibited a 2.8-fold increase in fatigue crack growth rate compared to the conventional material after heat treatment. The damage coefficients are 0.89 (iron), 0.67 (aluminium), 0.41 (nickel) and the formation of hydride and Ti3Al must be considered separately for AM titanium.

The following points should be further explored in future research: measurement of the binding energies and diffusivities of the traps on printed and post-processed microstructures; fatigue crack growth testing in pressurised gaseous hydrogen; explicit representation of the influence of porosity and residual stress in phase field models; and probabilistic calibration that takes process variability into predicted component life, so that simulation can aid the qualification of AM components for hydrogen service.

REFERENCES

[1] G. Álvarez, Z. Harris, K. Wada, C. Rodríguez, and E. Martínez-Pañeda, "Hydrogen embrittlement susceptibility of additively manufactured 316L stainless steel: Influence of post-processing, printing direction, temperature and pre-straining," *Addit. Manuf.*, vol. 78, no. 103834, 2023, doi: 10.1016/j.addma.2023.103834.

[2] A. Behvar, M. Haghshenas, and M. B. Djukic, "Hydrogen embrittlement and hydrogen-induced crack initiation in additively manufactured metals: A critical review on mechanical and cyclic loading," *Int. J. Hydrogen Energy*, vol. 58, pp. 1214–1239, 2024, doi: 10.1016/j.ijhydene.2024.01.232.

[3] C. Cui, R. Ma, and E. Martínez-Pañeda, "A generalised, multi-phase-field theory for dissolution-driven stress corrosion cracking and hydrogen embrittlement," *J. Mech. Phys. Solids*, vol. 166, no. 104951, 2022, doi: 10.1016/j.jmps.2022.104951.

[4] T. DebRoy *et al.*, "Additive manufacturing of metallic components – Process, structure and properties," *Prog. Mater. Sci.*, vol. 92, pp. 112–224, 2018, doi: 10.1016/j.pmatsci.2017.10.001.

[5] Z. Fu, P. Wu, Q. Yang, Q. Kan, and G. Kang, "Hydrogen-assisted fatigue crack propagation behavior of selective

laser–melted Inconel 718 alloy," *Corros. Sci. Art. no. 111745, 2023*, no. 111745, 2024, doi: 10.1016/j.corsci.2023.111745.

[6] R. P. Gangloff and B. P. Somerday, Eds., *Gaseous Hydrogen Embrittlement of Materials in Energy Technologies: Mechanisms, Modelling and Future Developments*, vol. 2. Woodhead Publishing, 2012. doi: 10.1533/9780857095374.

[7] R. P. Gangloff and B. P. Somerday, Eds., *Gaseous Hydrogen Embrittlement of Materials in Energy Technologies: The Problem, Its Characterisation and Effects on Particular Alloy Classes*, vol. 1. Woodhead Publishing, 2012. doi: 10.1533/9780857093899.

[8] D. Herzog, V. Seyda, E. Wycisk, and C. Emmelmann, "Additive manufacturing of metals," *Acta Mater.*, vol. 117, pp. 371–392, 2016, doi: 10.1016/j.actamat.2016.07.019.

[9] W. J. Sames, F. A. List, S. Pannala, R. R. Dehoff, and S. S. Babu, "The metallurgy and processing science of metal additive manufacturing," *Int. Mater. Rev.*, vol. 61, no. 5, pp. 315–360, 2016, doi: 10.1080/09506608.2015.1116649.

[10] A. Yadollahi and N. Shamsaei, "Additive manufacturing of fatigue resistant materials: Challenges and opportunities," *Int. J. Fatigue*, vol. 98, pp. 14–31, 2017, doi: 10.1016/j.ijfatigue.2017.01.001.

[11] S. P. Lynch, "Hydrogen embrittlement phenomena and mechanisms," *Corros. Rev.*, vol. 30, pp. 105–123, 2012, doi: 10.1515/corrrev-2012-0502.

[12] I. M. Robertson *et al.*, "Hydrogen embrittlement understood," *Metall. Mater. Trans. A*, vol. 46, no. 6, pp. 2323–2341, 2015, doi: 10.1007/s11661-015-2836-1.

[13] D. Sobola and R. Dallaev, "Exploring hydrogen embrittlement: Mechanisms, consequences, and advances in metal science," *Energies*, vol. 17, no. 12, 2024, doi: 10.3390/en17122972.

[14] H. Yu *et al.*, "Hydrogen embrittlement as a conspicuous material challenge—Comprehensive review and future directions," *Chem. Rev.*, vol. 124, no. 10, pp. 6271–6392, 2024, doi: 10.1021/acs.chemrev.3c00624.

[15] M. Khedr, A. Hamada, W. A. Elaziem, M. Jaskari, J. Kömi, and A. Järvenpää, "Effects of wall thickness variation on hydrogen embrittlement susceptibility of additively manufactured 316L stainless steel with lattice auxetic structures," *Materials (Basel).*, vol. 16, no. 6, 2023, doi: 10.3390/ma16062523.

[16] N. Pushilina *et al.*, "Hydrogen-induced phase transformation and microstructure evolution for Ti-6Al-4V parts produced by electron beam melting," *Metals (Basel).*, vol. 8, no. 5, 2018, doi: 10.3390/met8050301.

[17] C. Miehe, M. Hofacker, and F. Welschinger, "A phase field model for rate-independent crack propagation: Robust algorithmic implementation based on operator splits," *Comput. Methods Appl. Mech. Eng.*, vol. 199, no. 45–48, pp. 2765–2778, 2010, doi: 10.1016/j.cma.2010.04.011.

[18] C. Miehe, F. Welschinger, and M. Hofacker, "Thermodynamically consistent phase-field models of fracture: Variational principles and multi-field FE implementations," *Int. J. Numer. Methods Eng.*, vol. 83, no. 10, pp. 1273–1311, 2010, doi: 10.1002/nme.2861.

[19] J.-Y. Wu, V. P. Nguyen, C. T. Nguyen, D. Sutula, S. Sinaie, and S. P. A. Bordas, "Phase-field modeling of fracture," in *Advances in Applied Mechanics*, vol. 53, 2020, pp. 1–183. doi: 10.1016/bs.aams.2019.08.001.

[20] M. Isfandbod and E. Martínez-Pañeda, "A mechanism-based multi-trap phase field model for hydrogen assisted fracture," *Int. J. Plast.*, vol. 144, no. 103044, 2021, doi: 10.1016/j.ijplas.2021.103044.

[21] P. K. Kristensen, C. F. Niordson, and E. Martínez-Pañeda, "A phase field model for elastic-gradient-plastic solids undergoing hydrogen embrittlement," *J. Mech. Phys. Solids*, vol. 143, no. 104093, 2020, doi: 10.1016/j.jmps.2020.104093.

[22] E. Martínez-Pañeda, A. Golahmar, and C. F. Niordson, "A phase field formulation for hydrogen assisted cracking," *Comput. Methods Appl. Mech. Eng.*, vol. 342, pp. 742–761, 2018, doi: 10.1016/j.cma.2018.07.021.